Journal of Materials Chemistry

Cite this: J. Mater. Chem., 2011, 21, 12375

www.rsc.org/materials

PAPER

Tri-wing bismuth telluride nanoribbons with quasi-periodic rough surfaces†

Hang-Tian Zhu,[ab] Jun Luo,*[b] Hai-Ming Fan,[cd] He Zhang,[ab] Jing-Kui Liang,[be] Guang-Hui Rao,[b] Jing-Bo Li,[b] Guang-Yao Liu[b] and Zhen-Min Du[a]

Received 20th April 2011, Accepted 27th May 2011
DOI: 10.1039/c1jm11715g

Unique bismuth telluride nanostructures, tri-wing nanoribbons, are controllably synthesized on a large scale by a facile one-pot hydrothermal method. The length of the nanoribbon is up to tens of micrometres, and the wing of the nanoribbon is very thin with an average thickness of about 20 nm. During the synthesis process, tri-wing Te nanoribbons are first formed and act as the template, highly crystalline tri-wing Bi_2Te_3 nanoribbons are then obtained through a surface-directing diffusion process. An elaborate TEM study reveals a quasi-periodic rough surface with sequential $(1\bar{1}5)$ and $(\bar{1}05)$ planes along the Bi_2Te_3 nanoribbon, which is ascribed to the coherent growth of Bi_2Te_3 crystals during the surface-directing diffusion process. The successful synthesis of Bi_2Te_3 nanoribbons with rough surfaces opens up the opportunities of developing high performance nanoscale thermoelectrics as well as studying the surface state of Bi_2Te_3 nanoribbons as potential topological insulators.

Introduction

It has been demonstrated in recent years that the physical and chemical properties of quasi one-dimensional (1D) semiconductor materials can be significantly improved by specially designing the surface and interface structure of these materials. One notable example are rough Si nanowires with enhanced thermoelectric performance.[1] By introducing surface roughness and point defects during the growth, a dramatic reduction in thermal conductivity and a significant enhancement in the thermoelectric figure of merit (ZT) of Si nanowires are achieved. Similar novel phenomena have also emerged in a variety of 1D semiconductors such as supperlattice nanowires for advanced electronics[2,3] and hierarchical nanowire heterostructures for photonics.[4] In this context, the rational design and synthesis of 1D semiconductors with increasingly complex surface and interface structure are of importance in both fundamental research and practical applications. To meet this challenge, the development of a new approach for "dual-scale", *i.e.* both 1D shape and the surface and interface sub-structure, controlled synthesis in the nanoscale dimension, is urgently required.

Bismuth telluride (Bi_2Te_3) is the most widely used commercial thermoelectric material.[5,6] Recently, it has also been shown to have potential for the synthesis of a new class of topological insulators.[7–9] According to theoretical prediction,[10,11] 1D Bi_2Te_3 nanostructures with rough surfaces are expected to significantly improve thermoelectric performance through enhanced phonon scattering and quantum confinement effect. However, Bi_2Te_3, because of its anisotropic layered structure and weak van der Waals bonds between neighboring Te layers, usually grows into hexagonal nanoplatelets.[12–14] Although much effort has been made to fabricate 1D Bi_2Te_3 nanostructures, by methods such as electrodeposition with anodic porous alumina as the template,[15–18] catalyzed vapor-liquid-solid growth,[19,20] solvothermal/hydrothermal process,[21–23] and others,[24] the successful synthesis of impurity-free and highly crystalline 1D Bi_2Te_3 nanostructures on a large scale is rarely reported. Among the various methods used, sacrificed templates are commonly used to fabricate unique nanostructures where the template is consumed during the chemical reaction. In this method, nanoscale ion exchange and diffusion between the template and reactant play a vital role in morphology control and surface construction.[25] Rational selection of the template and reactant as well as the reaction conditions can effectively control the ion diffusion process, leading to many attractive nanostructures like CoSe nanorings,[26] gold nanoboxes,[27] $ZnAl_2O_4$ spinel nanotubes,[28] and so on. An attempt to use Te nanowires as a self-sacrificed template to synthesize telluride nanowires has also been reported.[29] However, it produces polycrystalline telluride nanowires which are undesirable for thermoelectric devices.

[a]*Department of Materials Science and Engineering, University of Science and Technology Beijing, Beijing, 100083, P. R. China*
[b]*Beijing National Laboratory for Condensed Matter Physics, Institute of Physics, Chinese Academy of Sciences, Beijing, 100190, P. R. China. E-mail: jluo@aphy.iphy.ac.cn*
[c]*School of Chemical Engineering, Northwest University, Xi'an, 710069, P. R. China*
[d]*School of Physics, National University of Ireland Galway, Galway, Ireland*
[e]*International Center for Materials Physics, Chinese Academy of Sciences, Shenyang, 110016, P. R. China*

† Electronic supplementary information (ESI) available: SEM image of tri-wing Bi_2Te_3 NRs synthesized on a large scale and indexed SAED pattern of a typical individual tri-wing Bi_2Te_3 NR. See DOI: 10.1039/c1jm11715g

In this report, we demonstrate that highly crystalline Bi_2Te_3 tri-wing nanoribbons (NRs) with quasi-periodic rough surfaces can be fabricated by a surface-directing diffusion process and coherent growth in a one-pot hydrothermal synthesis. Single-crystalline Te tri-wing NRs serving as both the precursor and sacrificed template are formed initially, a surface-directing diffusion process induced by their ultrathin wing structures occurs at a certain temperature, which in turn leads to the coherent growth of Bi_2Te_3 nanocrystals along the NR. The Bi_2Te_3 nanocrystal thus synthesized has both a 1D tri-wing structure and a quasi-periodic rough surface, opening up the opportunity of using it as a nanoscale building block for high performance integrated thermoelectric devices.

Experimental

Materials

Bismuth chloride ($BiCl_3$, 98%), potassium tellurite (K_2TeO_3, 98%), ethylenediaminetetraacetic acid disodium salt (EDTA, $C_{10}H_{14}N_2O_8Na_2 \cdot 2H_2O$, 99%), sodium hypophosphite monohydrate ($NaH_2PO_2 \cdot H_2O$, 98%), poly(vinyl alcohol) (PVA, 98–99% hydrolyzed) and sodium hydroxide (NaOH, 96%) were purchased from Sinopharm Chemical Reagent Co. Ltd. All the reagents were of analytical purity and used for synthesis without further purification.

Preparation of Bi_2Te_3 tri-wing NRs

In a typical experiment, 126 mg (0.4 mmol) $BiCl_3$ was dissolved in 40 ml of 20 mM EDTA aqueous solution to form Bi(III)-EDTA complex by continually stirring in order to stabilize the Bi^{3+} ions. After the addition of 5.3 g (50 mmol) $NaH_2PO_2 \cdot H_2O$ as the reducing agent and 123 mg PVA as surfactant, the pH value of the reaction solution was adjusted to 9 by the addition of NaOH. Then 102 mg (0.4 mmol) K_2TeO_3 was added and dissolved. The formed clear reactant solution was put into a 60 mL Teflon-lined stainless-steel autoclave, which was sealed and maintained at 140 °C for 12 h. After that, the container was cooled to room temperature naturally. The precipitates were collected by centrifugation and were washed several times with deionized water, and then dried at 60 °C overnight.

Characterization

Phase identification and structure analysis of the sample were carried out by X-ray powder diffraction (XRD) using a Rigaku D/max 2500 diffractometer with Cu-Kα radiation (50 kV × 250 mA) and a graphitic monochromator. The overview morphologies and sizes of the samples were obtained by a field-emission scanning electron microscope (FESEM), performed on a FEI-Sirion scanning electron microanalyzer and a Hitachi S-5200 ultra-high resolution scanning microscope. Transmission electron microscope (TEM) images, high resolution TEM (HRTEM) images, and selected area electron diffraction (SAED) patterns were recorded on a JEM-2010 transmission electron microscope using an accelerating voltage of 200 kV. The chemical composition and elemental mapping of the sample were analyzed by energy-dispersive X-ray (EDX) spectroscopy. Surface analysis using X-ray photoelectron spectroscopy (XPS) was carried out on a PHI Quantera SXM (ULVAC-PHI Inc., Japan) system using an Al-Kα (1486.6 eV) X-ray source.

Results and discussion

Synthetic strategy

The synthetic strategy for highly crystalline Bi_2Te_3 tri-wring NRs is illustrated in Fig. 1. The method employed here is a simple hydrothermal treatment of Bi(III)-EDTA and K_2TeO_3 in the presence of $NaH_2PO_2 \cdot H_2O$ and PVA at 140 °C for 12 h. $NaH_2PO_2 \cdot H_2O$ and PVA serve as reduction agent and surfactant, respectively. During the growth process, single-crystalline Te NRs are formed initially. Unlike Te nanowires, the wing surfaces of Te NRs are well defined and mainly surrounded by the (100) planes, which is closely related to its anisotropic crystal structure. The diffusion of Bi ions into Te NRs can only take place at a certain temperature and be directed by these (100) planes. A combination of this unique diffusion process and the anisotropic crystallographic structure of Bi_2Te_3 results in the coherent growth of Bi_2Te_3 with a quasi-periodic rough surface along the NR. The detailed experimental evidence is shown and discussed below. The idea presented here is to use ultrathin Te NRs with defined surfaces as the template for both 1D shape confinement and surface-directing diffusion to achieve a dual-scale controlled synthesis of Bi_2Te_3 tri-wing NRs. Despite the fact that it is well known that tuning the morphology of nanocrystals can acquire unique physical properties,[30] we show here that the particular morphology-dependent properties of the nanoribbon/nanobelt can be applied in a nanoscale template reaction to control the growth of 1D semiconductor nanostuctures with a desirable surface and interface.

Morphology and structure

The highly crystalline Bi_2Te_3 tri-wing NRs obtained on a large-scale (Fig. S1 in ESI†) have been examined by XRD, SEM and TEM. As can be seen from the XRD pattern shown in Fig. 2a, all the diffraction peaks can be exclusively indexed to the rhombohedral Bi_2Te_3 (JCPDS: 15-0863), and no other impurities are observed. The SEM images shown in Fig. 2b and 2c clearly reveal the rough surface and tri-wing structure of the Bi_2Te_3 NR which is composed of three wings with an angle of about 120° between each wing, and the average thickness of the wing is about 20 nm. The length of the NRs is up to tens of micrometres and the width of a single wing is about 150 nm. The TEM image and SAED pattern shown in Fig. 2d indicate that the Bi_2Te_3 tri-wing NRs are highly crystallized.

The local chemical composition and surface state of the sample were analyzed by EDX spectroscopy and XPS, respectively. As

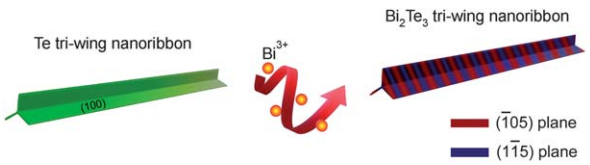

Fig. 1 Schematic illustration of the coherent growth of Bi_2Te_3 tri-wing NRs with Te NRs as the template.

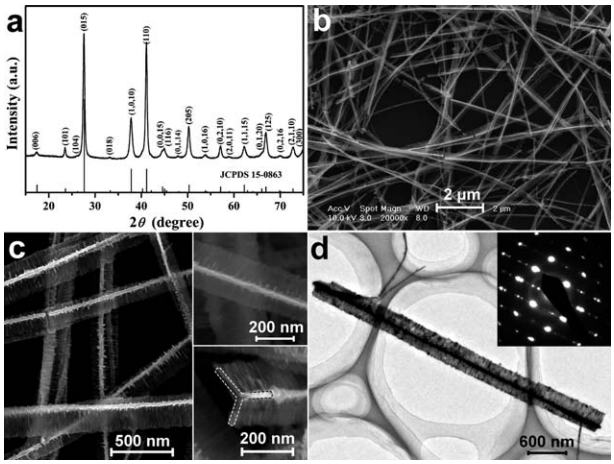

Fig. 2 (a) XRD pattern, (b) low- and (c) high-magnification SEM images, and (d) TEM image and SAED pattern of the as-prepared tri-wing Bi_2Te_3 NRs.

shown in Fig. 3a, the EDX spectrum of an individual NR reveals that the atomic ratio of Bi to Te is about 38.6 : 61.4, which is very close to 2 : 3. The EDX mapping shown in Fig. 3b indicates that the Bi and Te elements are distributed homogeneously in the tri-wing NR, which further confirms that the nanostructure is the Bi_2Te_3 compound. XPS results show that the peaks at 163.1, 157.6, 582.5 and 572.1 eV correspond to the binding energies of Bi $4f_{5/2}$, Bi $4f_{7/2}$, Te $3d_{3/2}$ and Te $3d_{5/2}$ of Bi_2Te_3,[31,32] respectively (Fig. 4). Additional peaks at 164.2, 158.9, 586.5 and 576.1 eV are in agreement with the XPS spectra of Bi $4f_{5/2}$, Bi $4f_{7/2}$, Te $3d_{3/2}$ and Te $3d_{5/2}$ from the oxide layer of Bi_2Te_3.[31,32] In addition to Bi and Te, the oxygen 1s peak is also observed in the XPS spectrum, indicating that the surface oxidation may take place after the sample is exposed to the atmosphere.[33]

Morphology and crystal structure evolution of nanocrystals have been investigated to elucidate the formation process of the Bi_2Te_3 tri-wing NRs. Fig. 5 and 6 show the XRD patterns and SEM images, respectively, of the sample at different reaction times. According to our experiments, the growth of Bi_2Te_3

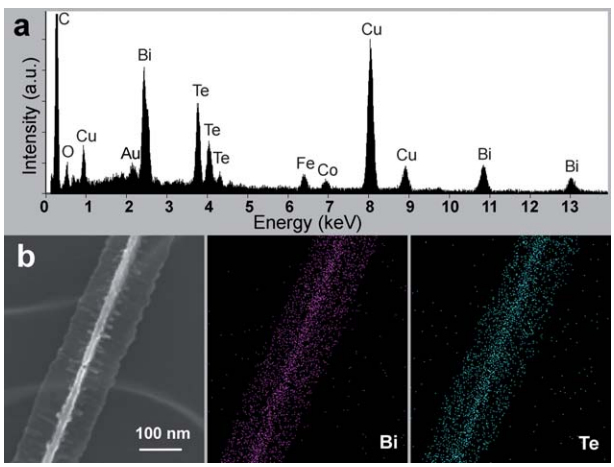

Fig. 3 (a) EDX spectrum and (b) SEM image with the corresponding EDX elemental mapping patterns of an individual tri-wing Bi_2Te_3 NR.

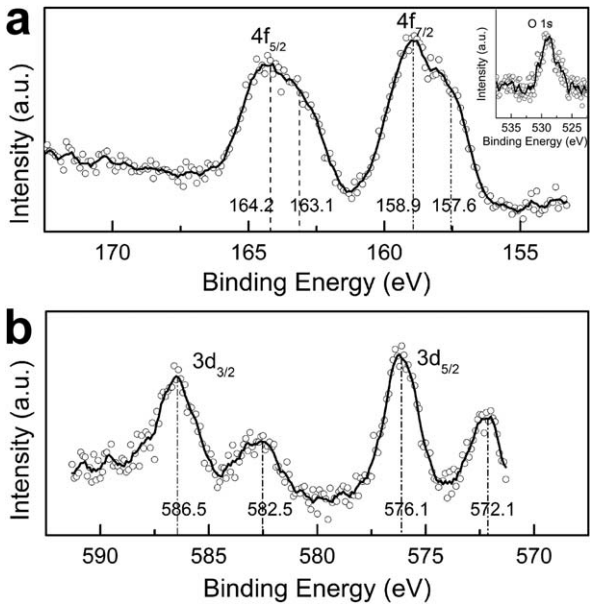

Fig. 4 (a) Bi 4f and (b) Te 3d XPS spectra of the Bi_2Te_3 tri-wing NRs. The inset of (a) shows the oxygen 1s peak. The circle and solid line denote the measured and smoothed XPS spectra, respectively.

tri-wing NRs can be divided into two stages. First, the Te tri-wing NRs with smooth surfaces are obtained within a reaction time of 2 h. Second, Bi_2Te_3 NRs with the same morphology but rough surfaces are gradually formed after 3 h. The formation of the 1D Te tri-wing NRs is, for the first time, reported here and can be ascribed to the anisotropic nature of the crystal structure. Since trigonal Te consists of helical chains of covalently bonded Te atoms which are bound together through van der Waals interactions, it has a strong tendency to form a 1D structure along the helical chain, *i.e.* the [001] direction (Fig. 7). This is consistent with our observation that the Te NRs formed at an early stage have a [001] growth direction (Fig. 8). However, the control experiments indicate that only Te nanowires or nanorods can be obtained without PVA, which eventually results in the polycrystalline Bi_2Te_3. Therefore, we believe that both the threefold symmetry of the t-Te crystallographic nature and

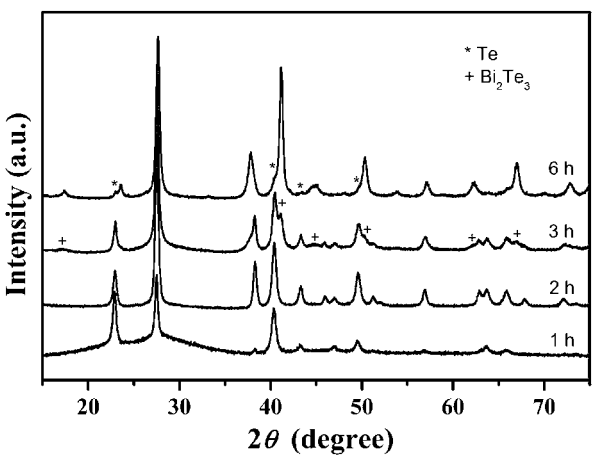

Fig. 5 XRD patterns of the sample with different reaction times.

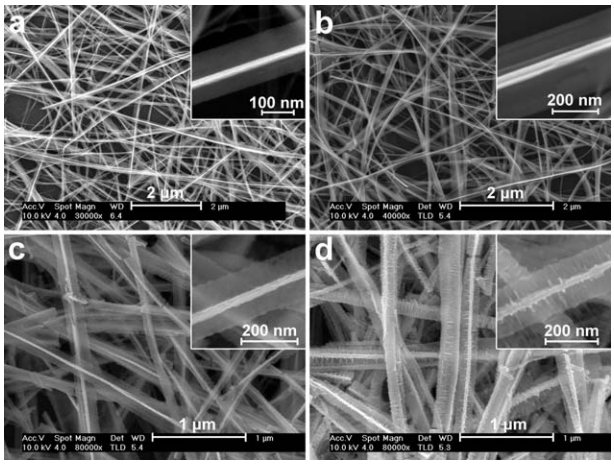

Fig. 6 SEM images of the sample with different reaction times. (a) 1 h, (b) 2 h, (c) 3 h, (d) 6 h.

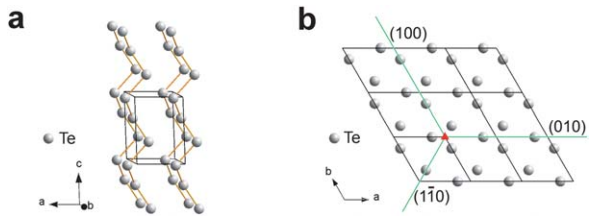

Fig. 7 (a) Crystal structure of trigonal Te showing the parallel helical chains held by van der Waals cohesion. (b) Projection of the trigonal Te crystal structure onto the *ab*-plane. The triangle denotes a trigonal axis. The proposed growth direction of the three wings is shown in panel b, and the angle between the tri-wing is 120°.

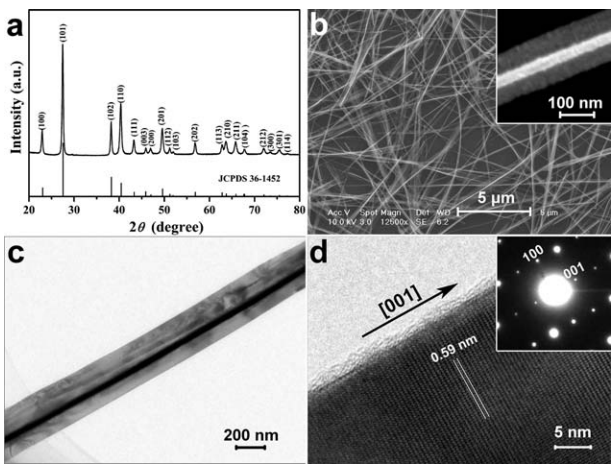

Fig. 8 (a) XRD pattern, (b) SEM image, (c) TEM image, and (d) HRTEM image and SAED pattern of tri-wing Te NRs.

polymer-controlled growth contribute to the formation of a tri-wing structure. On the one hand, Te prefers to grow into a structure with a threefold symmetry due to the inherent trigonal feature of its crystal structure as shown in Fig. 7b. On the other hand, PVA can kinetically control the growth rate of certain crystallographic facets of Te through selectively adsorbing on these facets, leading to a tailored crystal morphology.[34,35]

Besides, the (100) plane has much lower surface free energy than the other planes parallel to the [001] direction,[36,37] which prefers to grow into the wing structure with the assistance of PVA. The formation of tri-wing Te NRs at an early stage is crucial to the following template synthesis since they play roles in both shape confinement and ion diffusion control. In addition, it is worth mentioning that the reaction temperature is also an important parameter for the growth of Bi_2Te_3 nanostructures. It is found that the diffusion of Bi into Te nanoribbon could take place only when the temperature is higher than 120 °C. At a temperature lower than 100 °C, only Te NRs can be observed even after a reaction time of 12 h.

Growth mechanism

To further understand the formation of the quasi-periodic rough surface along the Bi_2Te_3 NR, the microstructure analysis of Bi_2Te_3 was carried out by TEM. The SAED pattern of the Bi_2Te_3 tri-wing NR shown in Fig. 2d is the superposition of two sets of diffraction spots with the same composition and crystal structure but different epitaxial orientation relationship. This microstructure feature is further confirmed by SAED patterns taken from other tri-wing NRs, and one of them is shown in Fig. 9a. The sharp diffraction spots match well with the calculated SAED pattern shown in Fig. 9b, while the weak ones are indexed as that shown in Fig. 9c. The corresponding TEM and HRTEM images of the individual NR are shown in Fig. 9d and 9e, respectively. The existence of two different crystallographic orientations is clearly demonstrated by the bright and dark areas shown in Fig. 9e. In the bright area, the spacing of 0.33 nm corresponds to the (1$\bar{1}$5) planes, and the (205) plane is perpendicular to the NR. In the dark area, the lattice fringes with a spacing of 1.02 nm correspond to the (003) planes of Bi_2Te_3, indicating that the [003] direction is along the NR. As shown in the inset of Fig. 9e, the lattice fringes of the (1$\bar{1}$5) planes extend to the dark area and coincide with the ($\bar{1}$05) planes, indicating a coherent growth of the two crystals. It should also be noted that the (1$\bar{1}$5) and ($\bar{1}$05) planes of Bi_2Te_3 not only have the same planar spacing but also the same atomic arrangement (Fig. 10). The coherent growth relationship is also demonstrated by the SAED pattern shown in

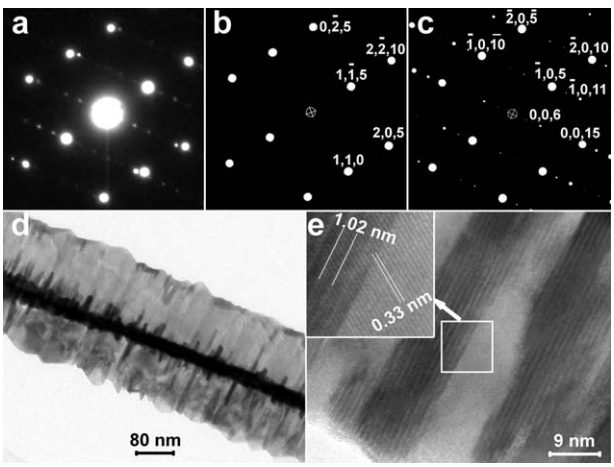

Fig. 9 (a) Measured and (b,c) calculated SAED patterns, (d) TEM image, and (e) HRTEM image of the tri-wing Bi_2Te_3 NR.

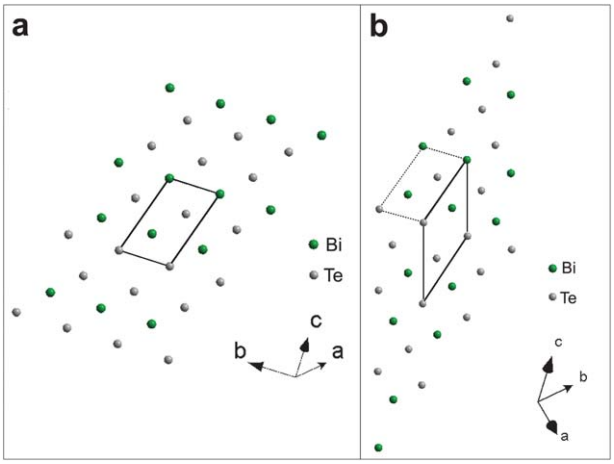

Fig. 10 Projections of the rhombohedral Bi_2Te_3 crystal structure onto the (a) $(\bar{1}05)$ and (b) $(1\bar{1}5)$ planes, respectively. The solid line shows the corresponding projection plane in a unit cell. The area marked by dashed line in $(1\bar{1}5)$ plane is the same as that onto the $(\bar{1}05)$ plane because the $(\bar{1}05)$ and $(1\bar{1}5)$ planes have the same atomic arrangement.

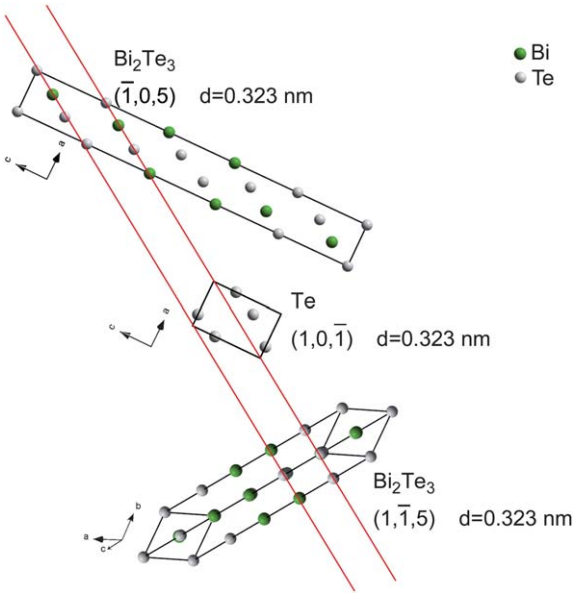

Fig. 11 Unit cells of Bi_2Te_3 (top and bottom) and Te (middle) showing the crystallographic orientation relationship of the coherent growth of Bi_2Te_3 with Te as the template, and the distance of the two parallel lines denotes their corresponding planar spacing.

Fig. 9a since the diffraction spots of $(1\bar{1}5)$ and $(\bar{1}05)$ are completely overlapped (see also Fig. S2 in the ESI†). On the basis of a series of TEM observations it can be concluded that the Bi_2Te_3 tri-wing NRs with quasi-periodic rough surfaces are formed with the Te tri-wing NRs as the template through a surface-directing ion diffusion process by which Bi cations diffuse into the Te nanostructures.

Although the detailed diffusion process is not well understood at this moment, a control experiment using a similar procedure with Te nanorods or nanowires as the templates results in Bi_2Te_3 nanoplatelets embedded partially in Te nanorods or a polycrystalline product, indicating that the surface-directing diffusion process by which Bi enters into the Te lattice through (100) planes does indeed contribute to the coherent growth of Bi_2Te_3 tri-wing NRs. In an earlier report, an epitaxial growth mechanism was suggested for the Bi_2Te_3 nanostrings which are formed through the epitaxial growth of Bi_2Te_3 nanoplatelets with Te nanorods as the template.[12] The Bi_2Te_3 nanoplatelets embedded partially in the Te nanorods are developed due to its anisotropic crystallographic structure, and the epitaxial orientation relationship is preserved to reduce the lattice mismatch energy.[12,38] In the current work, Bi_2Te_3 nanoplatelets are not observed, implying that the very thin wing structure is beneficial to the diffusion reaction. Similar to the formation of Bi_2Te_3 nanoplatelets, the Bi_2Te_3 tri-wing NRs also prefer to maintain the growth direction of the Te template. However, the growth of Bi_2Te_3 along the [001] direction is limited due to the lattice mismatch between Bi_2Te_3 and Te in this direction as well as its anisotropic layered structure. Therefore, the growth of Bi_2Te_3 along the [001] direction is interrupted and replaced by a low energy growth mode. As for the Te NRs template and the Bi_2Te_3 product, the $(10\bar{1})$ plane of Te and the $(1\bar{1}5)$ and $(\bar{1}05)$ planes of Bi_2Te_3 have almost the same interplanar spacing (Fig. 11), the coherent growth of Bi_2Te_3 along the $(1\bar{1}5)$ or $(\bar{1}05)$ plane is favorable in terms of energy minimization. Thus, it is reasonable to conclude that the growth kinetics and the intrinsic crystal properties of Bi_2Te_3 tri-wing NRs enable their coherent growth. And this coherent growth finally leads to a quasi-periodic rough surface. Moreover, further experiments involving other telluride NRs such as Ag_2Te NRs synthesized by the same procedure indicate that the principle reported here can be extended to the synthesis of many other 1D semiconductors with a quasi-periodic rough surface.

Conclusions

In summary, a dual-scale controlled synthesis of Bi_2Te_3 NRs with both tri-wing 1D shape and quasi-periodic rough surface on a large scale has been successfully achieved by a simple and one-pot hydrothermal method. The formation mechanism of such tri-wing Bi_2Te_3 NRs with complex surface and interface structure can be well explained by the self-sacrificed template reaction and the coherent growth along the NR. Te tri-wing NRs as the precursor are reported for the first time and are formed due to its trigonal crystal structure and the presence of PVA as a polymer-directing agent. Bi_2Te_3 tri-wing NRs with quasi-periodic rough surfaces are then obtained through a surface-directing ion diffusion and coherent growth process. Improved thermoelectric performance for the Bi_2Te_3 NRs is expected since the phonon scatting should be enhanced due to the rough surface, very thin tri-wing structure and coherent growth of Bi_2Te_3 crystals. We demonstrate here that by rational design and fabrication, the unique tri-wing structure obtained can be used as a template to control the growth of highly crystalline 1D nanostructures with an intricate surface and interface as well as enhanced physical properties. The principle and method developed in this work opens up the opportunity to fabricate other advanced functional materials for a variety of nanodevice applications.

Acknowledgements

This work was supported by the National Natural Science Foundation of China (Grant No. 11144002 and 21006079) and the National Basic Research Program of China (Grant No. 2007CB925003).

Notes and references

1 A. I. Hochbaum, R. K. Chen, R. D. Delgado, W. J. Liang, E. C. Garnett, M. Najarian, A. Majumdar and P. D. Yang, *Nature*, 2008, **451**, 163.
2 M. S. Gudiksen, L. J. Lauhon, J. F. Wang, D. C. Smith and C. M. Lieber, *Nature*, 2002, **415**, 617.
3 R. E. Algra, M. A. Verheijen, M. T. Borgström, L. F. Feiner, G. Immink, W. J. P. van Enckevort, E. Vlieg and E. P. A. M. Bakkers, *Nature*, 2008, **456**, 369.
4 F. Qian, Y. Li, S. Gradečak, H. G. Park, Y. J. Dong, Y. Ding, Z. L. Wang and C. M. Lieber, *Nat. Mater.*, 2008, **7**, 701.
5 R. Venkatasubramanian, E. Siivola, T. Colpitts and B. O'Quinn, *Nature*, 2001, **413**, 597.
6 B. Poudel, Q. Hao, Y. Ma, Y. Lan, A. Minnich, B. Yu, X. Yan, D. Wang, A. Muto, D. Vashaee, X. Chen, J. Liu, M. S. Dresselhaus, G. Chen and Z. Ren, *Science*, 2008, **320**, 634.
7 Y. L. Chen, J. G. Analytis, J. H. Chu, Z. K. Liu, S. K. Mo, X. L. Qi, H. J. Zhang, D. H. Lu, X. Dai, Z. Fang, S. C. Zhang, I. R. Fisher, Z. Hussain and Z. X. Shen, *Science*, 2009, **325**, 178.
8 R. Yu, W. Zhang, H. J. Zhang, S. C. Zhang, X. Dai and Z. Fang, *Science*, 2010, **329**, 61.
9 D. X. Qu, Y. S. Hor, J. Xiong, R. J. Cava and N. P. Ong, *Science*, 2010, **329**, 821.
10 L. D. Hicks and M. S. Dresselhaus, *Phys. Rev. B: Condens. Matter*, 1993, **47**, 16631.
11 M. S. Dresselhaus, G. Chen, M. Y. Tang, R. G. Yang, H. Lee, D. Z. Wang, Z. F. Ren, J. P. Fleurial and P. Gogna, *Adv. Mater.*, 2007, **19**, 1043.
12 W. Lu, Y. Ding, Y. Chen, Z. L. Wang and J. Fang, *J. Am. Chem. Soc.*, 2005, **127**, 10112.
13 W. Wang, B. Poudel, J. Yang, D. Z. Wang and Z. F. Ren, *J. Am. Chem. Soc.*, 2005, **127**, 13792.
14 W. D. Shi, L. Zhou, S. Y. Song, J. H. Yang and H. J. Zhang, *Adv. Mater.*, 2008, **20**, 1892.
15 A. L. Prieto, M. S. Sander, M. Martín-González, R. Gronsky, T. Sands and A. M. Stacy, *J. Am. Chem. Soc.*, 2001, **123**, 7160.
16 M. S. Sander, A. L. Prieto, R. Gronsky, T. Sands and A. M. Stacy, *Adv. Mater.*, 2002, **14**, 665.
17 M. Martín-González, A. L. Prieto, R. Gronsky, T. Sands and A. M. Stacy, *Adv. Mater.*, 2003, **15**, 1003.
18 L. Trahey, C. R. Becker and A. M. Stacy, *Nano Lett.*, 2007, **7**, 2535.
19 J. S. Lee, S. Brittman, D. Yu and H. Park, *J. Am. Chem. Soc.*, 2008, **130**, 6252.
20 F. Zhang, H. T. Zhu, J. Luo, J. K. Liang, G. H. Rao and Q. L. Liu, *Acta Phys. Sin.*, 2010, **59**, 7232.
21 Y. D. Li, J. W. Wang, Z. X. Deng, Y. Y. Wu, X. M. Sun, D. P. Yu and P. D. Yang, *J. Am. Chem. Soc.*, 2001, **123**, 9904.
22 A. Purkayastha, F. Lupo, S. Kim, T. Borca-Tasciuc and G. Ramanath, *Adv. Mater.*, 2006, **18**, 496.
23 G. Q. Zhang, Q. X. Yu, W. Wang and X. G. Li, *Adv. Mater.*, 2010, **22**, 1959.
24 J. Ham, W. Shim, D. H. Kim, S. Lee, J. Roh, S. W. Sohn, K. H. Oh, P. W. Voorhees and W. Lee, *Nano Lett.*, 2009, **9**, 2867.
25 S. C. Erwin, L. J. Zu, M. I. Haftel, A. L. Efros, T. A. Kennedy and D. J. Norris, *Nature*, 2005, **436**, 91.
26 Y. D. Yin, R. M. Rioux, C. K. Erdonmez, S. Hughes, G. A. Somorjai and A. P. Alivisatos, *Science*, 2004, **304**, 711.
27 Y. G. Sun and Y. N. Xia, *Science*, 2002, **298**, 2176.
28 H. J. Fan, M. Knez, R. Scholz, K. Nielsch, E. Pippel, D. Hesse, M. Zacharias and U. Gösele, *Nat. Mater.*, 2006, **5**, 627.
29 H. T. Zhu, H. Zhang, J. K. Liang, G. H. Rao, J. B. Li, G. Y. Liu, Z. M. Du, H. M. Fan and J. Luo, *J. Phys. Chem. C*, 2011, **115**, 6375.
30 Z. W. Wang, L. L. Daemen, Y. S. Zhao, C. S. Zha, R. T. Downs, X. D. Wang, Z. L. Wang and R. J. Hemley, *Nat. Mater.*, 2005, **4**, 922.
31 H. Bando, K. Koizumi, Y. Oikawa, K. Daikohara, V. A. Kulbachinskii and H. Ozaki, *J. Phys.: Condens. Matter*, 2000, **12**, 5607.
32 E. J. Menke, M. A. Brown, Q. Li, J. C. Hemminger and R. M. Penner, *Langmuir*, 2006, **22**, 10564.
33 S. S. Garje, D. J. Eisler, J. S. Ritch, M. Afzaal, P. O'Brien and T. Chivers, *J. Am. Chem. Soc.*, 2006, **128**, 3120.
34 Q. Xie, Z. P. Liu, M. W. Shao, L. F. Kong, W. C. Yu and Y. T. Qian, *J. Cryst. Growth*, 2003, **252**, 570.
35 S. L. Xiong, B. J. Xi, W. Z. Wang, C. M. Wang, L. F. Fei, H. Y. Zhou and Y. T. Qian, *Cryst. Growth Des.*, 2006, **6**, 1711.
36 X. L. Li, G. H. Cao, C. M. Feng and Y. D. Li, *J. Mater. Chem.*, 2004, **14**, 244.
37 J. Lu, Y. Xie, F. Xu and L. Y. Zhu, *J. Mater. Chem.*, 2002, **12**, 2755.
38 W. S. Wang, J. Goebl, L. He, S. Aloni, Y. X. Hu, L. Zhen and Y. D. Yin, *J. Am. Chem. Soc.*, 2010, **132**, 17316.

